

## Distribution of local Lyapunov exponents in spin-glass dynamics

S. L. A. de Queiroz\*

*Instituto de Física, Universidade Federal do Rio de Janeiro, Caixa Postal 68528, 21941-972 Rio de Janeiro RJ, Brazil*

R. B. Stinchcombe†

*Rudolf Peierls Centre for Theoretical Physics, University of Oxford, 1 Keble Road, Oxford OX1 3NP, United Kingdom*

(Received 16 March 2007; revised manuscript received 9 July 2007; published 16 November 2007)

We investigate the statistical properties of local Lyapunov exponents which characterize magnon localization in the one-dimensional Heisenberg-Mattis spin glass (HMSG) at zero temperature by means of a connection to a suitable version of the Fokker-Planck (FP) equation. We consider the local Lyapunov exponents (LLEs), in particular, the case of *instantaneous* LLE. We establish a connection between the transfer-matrix recursion relation for the problem and an FP equation governing the evolution of the probability distribution of the instantaneous LLE. The closed-form (stationary) solutions to the FP equation are in excellent accord with numerical simulations for both the unmagnetized and magnetized versions of the HMSG. Scaling properties for nonstationary conditions are derived from the FP equation in a special limit (in which diffusive effects tend to vanish), and also shown to provide a close description to the corresponding numerical-simulation data.

DOI: [10.1103/PhysRevB.76.184421](https://doi.org/10.1103/PhysRevB.76.184421)

PACS number(s): 05.10.Gg, 75.10.Nr, 63.20.Pw

### I. INTRODUCTION

The analytic treatment of quenched disordered systems in condensed-matter physics invokes many concepts from statistical theory. Among these, we shall be concerned in this paper with the connection between the probability distribution of Lyapunov characteristic exponents for the (equilibrium) problem of low-lying magnetic excitations in spin glasses, and the Fokker-Planck (FP) equation,<sup>1</sup> which is a key element in the description of nonequilibrium stochastic processes.

Links between an FP equation and stationary distributions of physical quantities in a transfer-matrix (TM) description have been established, usually in the context of calculating the probability distribution functions (PDFs) of electronic conductance in one-dimensional (1D) or quasi-1D noninteracting electronic systems with disorder (Anderson localization).<sup>2-9</sup> Specifically, one considers the distribution of the TM itself (or, equivalently, its transmission eigenvalues) between the left and right extremes of a wire of length  $L \gg 1$  lattice spacings. The FP equation is set up to account for the infinitesimal changes in the TM, caused by a small length variation  $\delta L$ . The quantities whose PDF is calculated are, therefore, aggregate in the sense that they explicitly incorporate all contributions for the TM, say, from  $x=0$  to  $L$ , i.e., they represent *global* Lyapunov exponents. This is in contrast with the approach we take here; as shown below, we shall concentrate on the PDF of *local* Lyapunov exponents, which appear not to have been as thoroughly exploited as their global counterparts (at least in the condensed-matter context of localization and similar problems).

As a model system to apply the ideas developed here, we consider spin waves (magnons) in a simplified spin glass model, the so-called Heisenberg-Mattis spin glass (HMSG).<sup>10</sup> In one dimension, the dynamics of HMSGs turns out to exhibit many nontrivial features,<sup>11-18</sup> including dynamic exponents,<sup>15,16,18</sup> different from the standard hydrodynamic predictions.<sup>19</sup>

In one dimension, all eigenstates are localized for any amount of disorder, though as energy  $\omega \rightarrow 0$ , the localization

length  $\lambda(\omega)$  diverges continuously. This, in turn, suggests the applicability of scaling concepts in the low-frequency, long-wavelength limit.

Operationally, one can obtain  $\lambda(\omega)$  in one-dimensional systems by using a TM approach and extract the smallest Lyapunov exponent (whose inverse corresponds to the largest localization length) which arises from repeated iteration of the TM. This has been done for HMSG chains,<sup>20-22</sup> and can be extended to HMSG in  $d=2$  and 3.<sup>18</sup>

Lyapunov exponents are well defined quantities in the sense that for  $N \gg 1$  iterations of the TM, the width of the distribution of their corresponding estimates shrinks to zero<sup>23</sup> (as  $N^{-1/2}$  in many cases of interest, as a consequence of the central limit theorem). However, it has been shown<sup>24-28</sup> that the so-called *local* Lyapunov exponents (LLE) (to be defined more accurately below) exhibit nontrivial distributions whose width remains finite even as  $N$  becomes fairly large (compared, e.g., with the localization length). Furthermore, LLEs may provide a wealth of information specific to the dynamics of the associated physical system, which does not manifest itself in the aggregated,  $\delta$ -function-like behavior of their global counterparts.

In this paper, we investigate the statistical properties of local Lyapunov exponents in the 1D HMSG at zero temperature by means of a connection to a suitable version of the FP equation.

In Sec. II, we recall pertinent aspects of the HMSG, specializing to one dimension. In Sec. III, we first consider the aggregate effects which characterize the (global) Lyapunov exponents for the system under study; then we investigate LLE, in particular the case of *instantaneous* LLE. We establish a connection between the TM-iterated recursion relation for the problem and a suitable FP equation governing the evolution of the probability distribution of the instantaneous LLE. We show that the closed-form (stationary) solutions to the FP equation are in excellent accord with numerical simulations for both the unmagnetized and magnetized versions of the 1D HMSG. Scaling properties for nonstationary con-

ditions are derived from the FP equation in a special limit (in which diffusive effects tend to vanish) and also shown to provide a close description to the corresponding numerical-simulation data. Finally, in Sec. IV, concluding remarks are made.

## II. HEISENBERG-MATTIS SPIN GLASSES: SCALING IN ONE DIMENSION

We consider Heisenberg spins on sites of a hypercubic lattice, with nearest-neighbor couplings

$$\mathcal{H} = - \sum_{\langle i,j \rangle} J_{ij} \mathbf{S}_i \cdot \mathbf{S}_j. \quad (1)$$

The bonds are randomly taken from a quenched, binary probability distribution,

$$P(J_{ij}) = p\delta(J_{ij} - J_0) + (1-p)\delta(J_{ij} + J_0). \quad (2)$$

Here, we shall mainly consider  $p=1/2$  (unmagnetized spin glass).

The Mattis model ascribes disorder to sites rather than bonds ( $J_{ij} \rightarrow J_0 \zeta_i \zeta_j$ ), so that the Hamiltonian reads

$$\mathcal{H}_M = - J_0 \sum_{\langle i,j \rangle} \zeta_i \zeta_j \mathbf{S}_i \cdot \mathbf{S}_j, \quad (3)$$

where  $\zeta_i = +1, -1$  with probability  $p, (1-p)$ . Then,  $p=1/2$  is the Mattis spin glass, while  $p \neq 1/2$  corresponds to a magnetized Mattis model. This way, the overall energy is minimized by making  $S_i^z = \zeta_i S$ , which constitutes a (classical) ground state of the Hamiltonian [Eq. (3)]. Consideration of the spin-wave equations of motion (see, e.g., Refs. 15, 16, and 18) gives, with  $\hbar=1$ ,

$$i\zeta_i du_i/dt = \sum_j J_0(u_i - u_j). \quad (4)$$

where the  $u_i$  are Mattis-transformed local (on-site) spin-wave amplitudes, and the sum is over sites  $j$  which are nearest neighbors of  $i$ . For the eigenmodes with frequency  $\omega$  (in units of the exchange constant  $J_0$ ), Eq. (4) leads to

$$\omega \zeta_i u_i = \sum_j (u_i - u_j). \quad (5)$$

The relationship of frequency to wave number  $k$  (in the context of localization, this corresponds to  $\lambda^{-1}$ ) at low energies is characterized by the dynamic exponent  $z$ ,

$$\omega \propto k^z. \quad (6)$$

For  $p=1/2$  in one dimension, it was predicted analytically<sup>15,16</sup> and verified by numerical calculations<sup>20-22</sup> that  $z=3/2$ . Still in one dimension, but at general  $p$ , Eq. (5) becomes

$$(2 - \zeta_i \omega) u_i = u_{i-1} + u_{i+1}. \quad (7)$$

A TM approach<sup>29,30</sup> can be formulated, giving<sup>15,16,20,21</sup>

$$\begin{pmatrix} u_{i+1} \\ u_i \end{pmatrix} = \begin{pmatrix} 2 - \zeta_i \omega & -1 \\ 1 & 0 \end{pmatrix} \begin{pmatrix} u_i \\ u_{i-1} \end{pmatrix} \equiv T_i(\omega) \begin{pmatrix} u_i \\ u_{i-1} \end{pmatrix}. \quad (8)$$

The procedure for calculating Lyapunov exponents in this case is the same as that used for Anderson localization

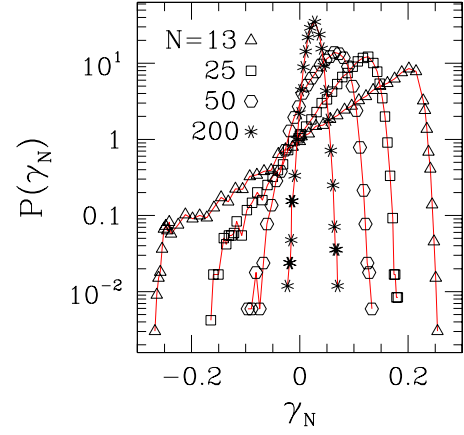


FIG. 1. (Color online) Normalized histograms of occurrence of LLE  $\gamma_N$  for  $p=1/2$  (spin glass) and for several values of  $N$ . For each histogram,  $N_s=10^5$  samples were taken. Here,  $\omega=0.015$ .

problems.<sup>29</sup> Indeed, in both cases the TM is symplectic, and one can use Oseledec's theorem and dynamic filtration<sup>23</sup> to extract the smallest Lyapunov exponent, whose inverse is the largest localization length.

## III. LYAPUNOV EXPONENTS

### A. Aggregate effects: The $N \rightarrow \infty$ limit

The Lyapunov exponent emerging from iteration of Eq. (8) is given by

$$\gamma(\omega) = \lim_{N \rightarrow \infty} \frac{1}{N} \ln \left\| \left( \prod_{i=1}^N T_i(\omega) \right) |v_0\rangle \right\|, \quad (9)$$

where

$$|v_0\rangle \equiv \begin{pmatrix} u_1 \\ u_0 \end{pmatrix}$$

is an arbitrary initial vector of unit modulus.

The LLE,  $\gamma(N, \omega)$ , is defined<sup>24-28</sup> as the finite- $N$  version of Eq. (9). For the sake of completeness, before going further we exhibit the evolution of the statistics of  $\gamma(N, \omega)$  (hereafter referred to as  $\gamma_N$  for short) against increasing  $N$ . We consider the TM given in Eq. (8), with  $p=1/2$  and  $\omega=0.015$  (fixed), for which case the existing numerical results<sup>18,20,21</sup> give  $\lambda \approx 57$  lattice spacings, i.e.,  $\gamma \approx 0.0175$ .

In Fig. 1, one sees that the PDF,  $P(\gamma_N)$ , of  $\gamma_N$  takes on an approximately Gaussian shape only for  $N \geq \lambda$ . Figure 2(a) provides a quantitative check on the increasing narrowness of the PDF for  $N \geq \lambda$  and on the convergence process  $\langle \gamma_N \rangle \rightarrow \gamma$ . One can infer the accuracy of the single-sample estimate corresponding to  $N=10^7$  [denoted by an arrow pointing to the vertical axis in Fig. 2(a)] by extrapolating the  $N$  dependence of the width  $\Delta_N$  of the PDF against  $N \leq 51$  200 (shown in the main diagram). The result is  $\gamma=0.01752(4)$ : hence, the associated error bar would be invisible on the scale of the figure.

The simplest quantitative indicator of whether the PDF actually turns Gaussian with increasing  $N$  (in the process of

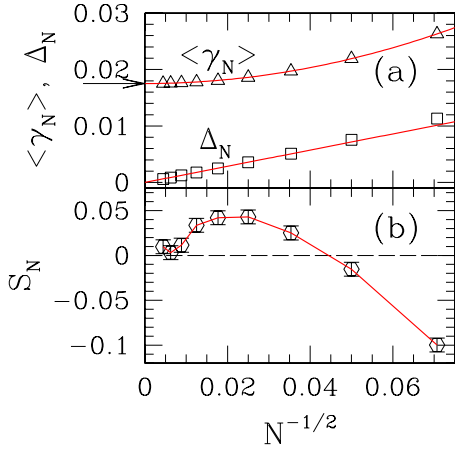


FIG. 2. (Color online) Estimates from the statistics of LLE  $\gamma_N$  data for  $N=2^k \times 100$ ,  $k=1, \dots, 9$ , against  $N^{-1/2}$ . For each  $N$ ,  $N_s = 10^5$  samples were taken. Here,  $p=1/2$  and  $\omega=0.015$ . (a) Mean values  $\langle \gamma_N \rangle$  and rms deviations  $\Delta_N$ . Arrow on vertical axis indicates estimate from a single sample, with  $N=10^7$ . Full lines are, respectively, quadratic ( $\langle \gamma_N \rangle$ ) and linear ( $\Delta_N$ ) fits of data; the latter taking only  $N \geq 800$  into account. (b) Skewness  $S_N$ . Error bars correspond to incompletely sampled Gaussian distributions with  $N_s=10^5$  (see text).

becoming a  $\delta$  function, characteristic of the self-averaging property just demonstrated) is its skewness,<sup>31</sup>  $S_N \equiv \langle [(\gamma_N - \langle \gamma_N \rangle) / \Delta_N]^3 \rangle$ . One must bear in mind that because the number of samples  $N_s$  is finite (incomplete sampling),  $S_N$  itself will have a distribution. While this is true also for  $\langle \gamma_N \rangle$  and  $\Delta_N$ , the effects on  $S_N$  are much more prominent since it is the ratio of two quantities which, in the present case, both vanish as  $N, N_s \rightarrow \infty$ . Indeed, we have checked that for the data shown in Fig. 2(a), corresponding to  $N_s=10^5$ , estimates of  $\langle \gamma_N \rangle$  and  $\Delta_N$  from distinct sequences of pseudorandom numbers usually differ only by a few parts in  $10^4$ . On the other hand, it is known<sup>31</sup> that for an incompletely sampled Gaussian distribution, the width of its own skewness distribution is approximately  $\sqrt{6/N_s}$  ( $\approx 0.0078$  here). Since our own large- $N$  PDFs are, to zeroth order, Gaussian, we shall use this value as a lower bound to the uncertainty of our estimates for  $S_N$ . The results are displayed in Fig. 2(b). Given the trend exhibited by the calculated  $S_N$  for the three largest values of  $N$  used (especially in contrast with the smaller- $N$  region), it appears safe to conclude that the skewness is in fact approaching zero, within the pertinent error bars. Thus, the overall evidence is compatible with a limiting Gaussian form for the PDF of the LLEs as  $N \rightarrow \infty$ .

### B. Local effects and the Fokker-Planck equation

We now turn to the opposite limit, which is our main concern here. Instead of considering the aggregate effect of contributions to  $\gamma_N$ , we shall analyze the PDFs of such contributions separately.

The case  $N=1$  of Eq. (9) is often denoted as “instantaneous” LLE.<sup>28</sup> Here, we shall use the term in the following way. The instantaneous LLE at  $i=M$ , to be denoted by  $s(M)$ ,

is the local contribution to the LLE, given at  $i=M$ , of the multiplying process denoted in Eq. (9). One then has

$$\gamma_N = \frac{1}{N} \sum_{M=1}^N s(M). \quad (10)$$

For a one-dimensional mapping, the instantaneous LLE, as defined above, would be simply the local stretch factor.<sup>28</sup> In the present case, where even in one dimension the TM is  $2 \times 2$ , it is known that the eigenvectors (Lyapunov basis) of a product of random matrices are only *local* properties, as opposed to the corresponding eigenvalues (i.e., the Lyapunov spectrum) which are global ones.<sup>23</sup> Thus, one has a rotation of the local Lyapunov basis as the TM is repeatedly iterated. As the TM is symplectic, in one dimension this means that the (two) local eigenvalues are inverse of each other, so  $s(M)$  can be extracted by suitable analysis of the growth factor associated with a given member of the Lyapunov basis.

The connection with the FP equation proceeds as follows. One gets, by taking the continuum limit of Eq. (7),

$$\omega \zeta(\ell) u(\ell) = \frac{\partial^2 u(\ell)}{\partial \ell^2}, \quad (11)$$

where  $\ell$  stands for position along the axis. One sees that  $u(\ell)$  is the result of accumulated contributions from the instantaneous Lyapunov exponent  $s(\ell')$ ,  $0 \leq \ell' \leq \ell$ ,

$$u(\ell) = \exp\left(\int_0^\ell s(\ell') d\ell'\right). \quad (12)$$

Therefore, the right-hand side of Eq. (11) turns into

$$\frac{\partial^2 u(\ell)}{\partial \ell^2} = \left(s^2(\ell) + \frac{\partial s(\ell)}{\partial \ell}\right) u(\ell). \quad (13)$$

Equation (11) then yields the following equation for the stochastic variable  $s(\ell)$ :

$$s^2(\ell) + \frac{\partial s(\ell)}{\partial \ell} = \omega \zeta(\ell). \quad (14)$$

In general case,  $\zeta$  is a binary-distributed variable with mean  $\mathcal{M}_1=2p-1$  and variance  $\mathcal{M}_2=4p(1-p)$ . The FP equation corresponding to the evolution of the probability distribution of  $s$  is, with  $\ell$  naturally assuming the role of timelike variable,<sup>1</sup>

$$\frac{\partial P(s, \ell)}{\partial \ell} = \frac{\partial}{\partial s} [s^2 + \omega \mathcal{M}_1] P(s, \ell) + \frac{1}{2} \frac{\partial^2}{\partial s^2} [\mathcal{M}_2 \omega^2] P(s, \ell). \quad (15)$$

### C. Unmagnetized Heisenberg-Mattis spin glass

In this section, we take the special case of an unmagnetized HMSG ( $p=1/2$ ). Equation (15) then becomes

$$\frac{\partial P(s, \ell)}{\partial \ell} = \frac{\partial}{\partial s} [s^2 P(s, \ell)] + \frac{1}{2} \frac{\partial^2}{\partial s^2} [\omega^2 P(s, \ell)]. \quad (16)$$

Assuming stationarity,  $P(s, \ell) \rightarrow P(s)$  (which corresponds to the regime  $\ell \geq \lambda$ ), the equation to solve is

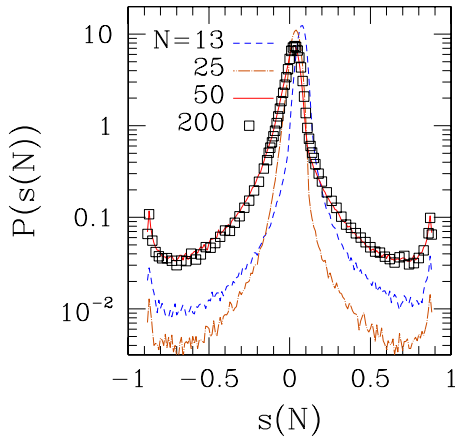


FIG. 3. (Color online) Normalized histograms of occurrence of instantaneous LLE  $s(N)$  for several values of  $N$ . For each histogram,  $N_s=10^6$  samples were taken. Here,  $p=1/2$  and  $\omega=0.015$ .

$$\frac{\partial}{\partial s}[s^2 P(s)] + \frac{1}{2} \frac{\partial^2}{\partial s^2}[\omega^2 P(s)] = 0. \quad (17)$$

Thus, one gets

$$P(s) = \tilde{C} \exp(-2s^3/3\omega^2) \int_{-\infty}^s \exp(2y^3/3\omega^2) dy. \quad (18)$$

It is immediate to see that the  $3/2$  power, referred to in connection with Eq. (6), arises in the scaling variable. Furthermore, it is clear from the derivation of the present results that they apply only in the scaling regime, i.e.,  $\omega \rightarrow 0$ , small  $|s|$ ,  $\ell \gtrsim \lambda$ .

With  $\int_{-\infty}^{\infty} dy \int_{-\infty}^y dx \exp(x^3 - y^3) \equiv C_0 \approx 4.8$ , the normalization of Eq. (18) implies

$$\tilde{C} = \tilde{C}(\omega) = \frac{1}{(3\omega^2/2)^{1/3} C_0}. \quad (19)$$

The numerical verification of the ideas just presented begins by checking the behavior of the PDFs for  $s(N)$  against varying  $N$ . Selected data are shown in Fig. 3. One can see that for the ranges of  $N$  considered in the figure, the overall shape of the PDFs remains roughly constant, though a slight narrowing and shifting of the central peak take place as  $N$  increases. This is in contrast with the LLEs exhibited in Fig. 1, for which variation of  $N$  in the same range was accompanied by a pronounced change in shape and width of the respective PDFs. For  $1 \leq N \leq 13$  (not shown in the figure), the PDF for  $s(N)$  starts nearly flat at  $N=1$  and gradually develops both the central peak and the small “wings” at the ends (whose relevance in Fig. 3 is overemphasized by the logarithmic scale on the vertical axis). The very good superposition of the  $N=50$  and  $200$  data in the figure indicates the predicted trend toward a fixed,  $N$ -independent form, which corresponds to stationarity of the FP equation [see Eq. (17)]. This has been confirmed by examination of numerical PDFs for  $100 \leq N \leq 600$ . Recalling that the localization length for

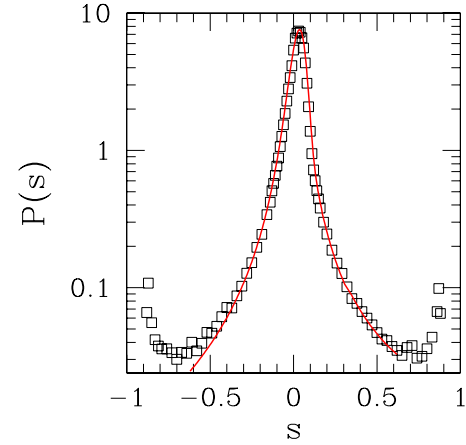


FIG. 4. (Color online) Squares: normalized histogram of occurrence of instantaneous LLE  $s$  from  $N_s=10^6$  samples for  $N=200$ ,  $p=1/2$ , and  $\omega=0.015$ . Continuous line is the analytical form, Eq. (18), normalized and with appropriate scaling of variables [see also Eq. (19)].

$\omega=0.015$ , as is the case of Fig. 3, is  $\lambda \approx 57$  lattice spacings, we see that the condition for an  $N$ -independent PDF is indeed  $N \gtrsim \lambda$ .

We now test whether the form given in Eq. (18) describes our numerical data. Figure 4 shows that the agreement is excellent in the region  $-0.5 \leq s \leq 0.5$ , which is where scaling is expected to hold. Note that there are no adjustable parameters in the fit, all scale factors being provided by normalization and scaling considerations.

In Fig. 5, we test for consistency of scaling among numerical data for different energies  $\omega$ , as suggested by Eq. (18). Again, the agreement with predictions is excellent, provided that the conditions upon which Eq. (18) was derived are obeyed.

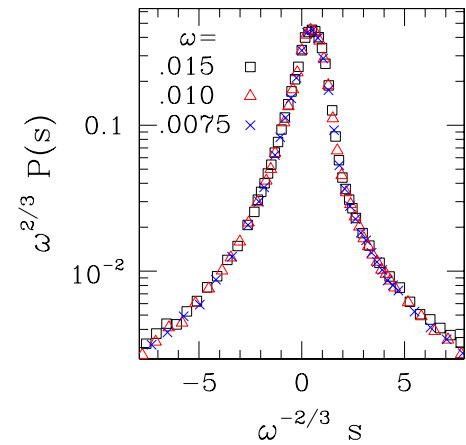


FIG. 5. (Color online) Scaling plots of normalized histograms of occurrence of instantaneous LLE, as suggested by Eq. (18) for assorted energies. In all cases,  $p=1/2$ ,  $N_s=10^6$  samples, and  $N=200$  [so the condition  $N \gtrsim \lambda(\omega)$  is always obeyed].

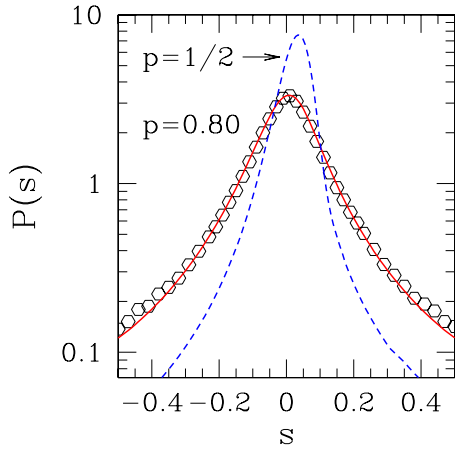


FIG. 6. (Color online) Hexagons: normalized histogram of occurrence of instantaneous LLE  $s$  from  $N_s=10^6$  samples for  $\omega=0.015$  and  $p=0.80$  (here, we used  $N=600$ , as the localization length is  $\lambda \approx 498$ ). Continuous line is the analytical form [Eq. (20)] normalized. The dashed line is the analytical result for  $p=1/2$  from Eq. (18).

#### D. Magnetized Heisenberg-Mattis spin glass ( $p \neq \frac{1}{2}$ )

For the magnetized case  $p \neq 1/2$ , we return to the general form of the FP equation [Eq. (15)], whose stationary solution is given by

$$P(s) = \tilde{C}' \exp[-f(s)] \int_{-\infty}^s \exp[f(y)] dy, \quad (20)$$

where

$$f(y) = f(y, \omega, p) = \frac{1}{\omega^2 \mathcal{M}_2} \left( \frac{2y^3}{3} + 2\omega \mathcal{M}_1 y \right). \quad (21)$$

In analogy with Sec. III C, we first check whether Eq. (20) gives a faithful description of simulational data for given  $p$  and  $\omega$ . In Fig. 6, the calculated data for  $p=0.8$  and  $\omega=0.015$  are shown together with the analytical result from Eq. (20) for the same values of  $p$  and  $\omega$ . Apart from an overall normalization factor which affects only the vertical scale, there are no adjustable parameters. Again, the agreement is very good.

In order to emphasize the degree to which the shape and range of the PDFs are affected by variations in the physical parameters, Fig. 6 also shows the PDF for the unmagnetized case at the same energy  $\omega=0.015$ . As  $p$  increases from  $1/2$ , the general trend is toward the reduction of the skewness [which is  $\approx -0.32$  at  $p=1/2$ ,  $-0.02$  at  $p=0.80$ , and (in absolute value)  $<0.01$  at  $p=0.95$ ]. The peak of the distribution, which is about one standard deviation away from the origin at  $p=1/2$ , approaches  $s=0$  as  $p$  approaches unity. This process is accompanied by a broadening of the PDF.

We now proceed to framing the preceding observations within a crossover description. One sees that because  $f(y)$  in Eq. (21) is a polynomial in  $y$  for  $p \neq 1/2$ , it is not possible to develop scaling arguments (over the whole range of the variable  $s$ ) similar to those invoked for  $p=1/2$ , and graphically depicted in Fig. 5. Nevertheless, analysis

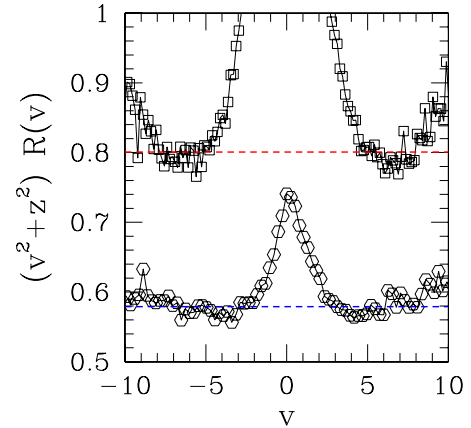


FIG. 7. (Color online) Symbols are data from normalized histograms of occurrence of instantaneous LLE  $s$  from  $N_s=10^6$  samples, plotted as suggested by Eq. (22) [see text for definitions of  $z$ ,  $v$ , and  $R(v)$ ]. Hexagons:  $p=0.8$  and  $\omega=0.0075$  ( $z \approx 2.03$ ); and squares:  $p=0.95$  and  $\omega=0.015$  ( $z \approx 3.32$ ). Horizontal lines mark the central estimates of averages of  $(v^2+z^2)R(v)$ , respectively, along  $-9 < v < -3$  (lower) and  $-8 < v < -4$  (upper).

of Eq. (21) shows that the crossover away from unbiased ( $p=1/2$ ) behavior is governed by the dimensionless ratio  $z \equiv (\omega \mathcal{M}_1)^{1/2} / (\omega^2 \mathcal{M}_2)^{1/3} (\approx [(p-1/2)/\omega^{1/3}]^{1/2})$  away from  $p \rightarrow 1$ ). This way,  $s$  scales with  $\omega^{2/3}$  for  $z \ll 1$  and with  $\omega/(p-1/2)$  for  $z \gg 1$ . Analysis of the asymptotic behavior of  $P(s)$ , as given by Eqs. (20) and (21), shows that, with  $z$  defined as above and  $v \equiv s\omega^{-2/3}$ , one has for the tails of the distribution,

$$R(v) \sim \frac{C}{v^2 + z^2} \quad |v| \gg 1, \quad (22)$$

where  $R(v) \equiv \omega^{2/3} P(s)$  and (for  $z \gg 1$ ) the normalization constant  $C \propto z$ .

Numerical checks of Eq. (22) against simulational data must be carried out for suitable ranges of  $p$ ,  $\omega$ , and  $s$  (equivalently,  $z$  and  $v$ ) such that (i) asymptotic behavior has already set in (i.e., large  $|s|$  and  $|v|$ ) and (ii) one is still within the scaling regime (which implies small  $|s|$ ). Thus, one expects Eq. (22) to hold only within windows of varying width, which may or may not be easy to identify against statistical noise.

In Fig. 7, we show that it is indeed possible to find intervals of  $v$  along which a plot of  $(v^2+z^2)R(v)$  is rather flat, as suggested by Eq. (22). While the evidence is somewhat smeared for the upper set of data (corresponding to  $p=0.95$  and  $\omega=0.015$ , i.e.,  $z_1 \approx 3.32$ ), it is clear for the lower one (for which  $p=0.80$  and  $\omega=0.0075$ , i.e.,  $z_2 \approx 2.03$ ). Furthermore, the ratio of the averages of  $(v^2+z^2)R(v)$  (each denoted by a horizontal line in the figure) along the respective flat sections (these latter defined with an inevitable degree of arbitrariness) is  $\approx 1.4(1)$ . This compares reasonably well with the predicted value  $z_1/z_2=1.64$  [see Eq. (22) and the comments immediately below it]. Given that the latter result is expected to hold for  $z \gg 1$ , one may infer that the small discrepancy found is due to  $z_1$  and  $z_2$  not being large enough.

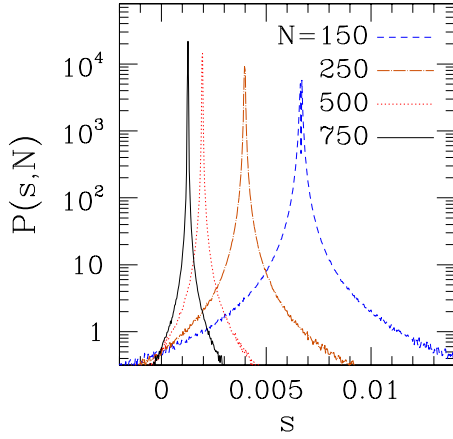


FIG. 8. (Color online) Central sections of normalized histograms of occurrence of instantaneous LLE  $s$  from  $N_s = 10^7$  samples for  $\omega = 10^{-6}$ ,  $p = 0.60$ , and  $N$  as indicated.

Finally, we remark that the pure-ferromagnet limit is somewhat subtle, because in order to reach the stationary regime of the FP equation where the  $N$ -independent PDF forms hold, the condition  $N \geq \lambda$  must be obeyed. However, as  $p \rightarrow 1$  and for the low energies where scaling is valid,  $\lambda$  diverges as one approaches the pure-system magnon band (located at  $0 \leq \omega < 2$  in the current units). For example, at  $p = 0.95$  and  $\omega = 0.015$ , one gets  $\lambda \approx 2500$ .

### E. Nonstationary regime for $p \neq \frac{1}{2}$

Still for the magnetized case  $p \neq 1/2$ , one can learn more by considering selected aspects of the nonstationary regime. Going back to Eq. (15), one sees that in the limit  $p - 1/2 \gg \omega^{1/3}$ , i.e.,  $z \gg 1$ , the diffusive term becomes small and this regime is associated with just streaming in leading order. The nonstationary equation to be solved is thus

$$\frac{\partial P(s, \ell)}{\partial \ell} = \frac{\partial}{\partial s} [(s^2 + \omega \mathcal{M}_1) P(s, \ell)]. \quad (23)$$

With  $\beta \equiv [\omega(p - 1/2)]^{1/2}$ ,  $\tilde{t} \equiv \ell \beta$ ,  $\tilde{y} \equiv s/\beta$ , and defining  $Q(\tilde{t}, \tilde{y})$  such that  $Q(\tilde{t}, \tilde{y}) d\tilde{y} = P(s, \ell) ds$ , Eq. (23) turns into

$$\frac{\partial Q}{\partial \tilde{t}} = \frac{\partial}{\partial \tilde{y}} (\tilde{y}^2 + 1) Q, \quad (24)$$

whose general solution is

$$Q(\tilde{t}, \tilde{y}) = \frac{1}{1 + \tilde{y}^2} f(\tilde{t} + \tan^{-1} \tilde{y}). \quad (25)$$

In order to have the condition  $p - 1/2 \gg \omega^{1/3}$  fulfilled to a good extent, so that the scaling behavior predicted by Eq. (25) could be unequivocally demonstrated, we used  $p = 0.6$  and  $\omega = 10^{-6}$ . For such a choice, the localization length is  $\lambda \geq 4 \times 10^4$ . This allowed us to take values of  $N$  equal to several hundred lattice spacings, which are both much larger than unity (so discrete-lattice effects are negligible) and still much shorter than  $\lambda$  (thus guaranteeing nonstationarity by a broad margin). Figure 8 shows the region close to the central

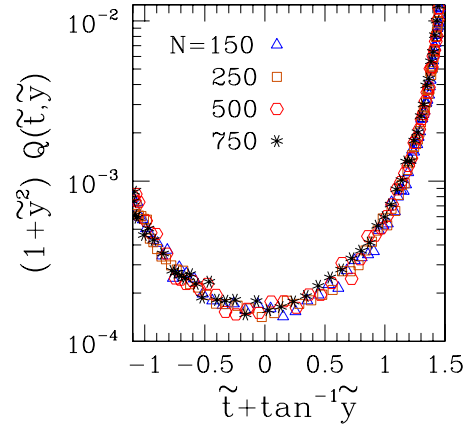


FIG. 9. (Color online) Scaling plot of data displayed in Fig. 8, as suggested by Eq. (25).

peaks of the PDFs (where scaling is expected to hold) for  $N = 150, 250, 500$ , and  $750$ . In Fig. 9, the same data are shown in a scaling plot, as suggested by Eq. (25). Note that the number of samples  $N_s$  is 1 order of magnitude larger than, e.g., that used in earlier sections of this work. This was necessary, in view of the relatively wide scatter of the PDFs: typically, they displayed almost flat tails running out to  $|s| \geq 0.07$ , so the relevant data as far as scaling is concerned were a small subset of the total gathered (compare the horizontal scale in Fig. 8). Even so, one can see, close to the bottom of the scaling curve in Fig. 9, that a non-negligible degree of fluctuation-induced spread still remains. Nevertheless, the overall agreement with the scaling predictions of Eq. (25) is remarkable.

## IV. DISCUSSION AND CONCLUSIONS

We have investigated scaling properties of the PDFs of Lyapunov exponents for the one-dimensional Heisenberg-Mattis spin glass.

In Sec. III A, we showed that for a given energy  $\omega$  [small enough, such that the localization length  $\lambda(\omega)$  is sufficiently large for scaling concepts to apply], the PDF of the LLE  $\gamma(N, \omega)$  takes on a shape which, for  $N \geq \lambda(\omega)$ , is increasingly close to a Gaussian. In the limit  $N \rightarrow \infty$ , the PDFs turn into  $\delta$  functions, in conformity with the central limit theorem. Thus, such aggregate effects reflect only general statistical properties of fluctuations in systems with many (almost) independent degrees of freedom. The connection with the underlying physical problem is traced exclusively through the dependence of the numerical value of the (asymptotic) Lyapunov exponent with energy (and ferromagnetic bond concentration; though this latter aspect was not exploited here, it has been investigated before<sup>20-22</sup>).

On the other hand, the PDFs for the instantaneous Lyapunov exponents, as defined via Eq. (10), display the following properties of interest, exhibited in Secs. III B–III D: (i) for  $N \geq \lambda(\omega)$  they approach a fixed, nontrivial shape with nonvanishing width, (ii) such specific shape can be predicted through a connection with the stationary state of

an FP equation, and (iii) the shape is a “fingerprint” shared by all the systems in the universality class in which the statistical properties of the system lie. Furthermore, the FP equation providing the link can be set up directly from, and closely reflects, the physical features of the system under investigation [see especially Eqs. (11)–(16)].

The applicability of a description via an FP equation goes beyond the stationary state, as shown in Sec. III E. There, it is shown that the scaling of nonstationary PDFs in a specific regime (in which diffusion effects are expected to be negligible) closely follows predictions drawn from the corresponding form of the FP equation.

In the present work, we have demonstrated that an FP approach can be successively applied to both stationary and nonstationary properties of the PDF of instantaneous Lyapunov exponents for Heisenberg-Mattis spin glasses.

As a final remark, we believe that the scaling properties of the PDF of Lyapunov exponents described here are identical to those pertinent to the zero-temperature random-bond ( $\pm 1$ ) classical Heisenberg chain. This comes via the identification of the scaling properties of the low-energy excitations of the HSMG chain with those of the classical Heisenberg model in

one dimension<sup>15,16,20,21</sup> plus the general applicability of the FP equation in the continuum.<sup>1</sup>

It is expected that treatments along these lines can be devised, with similar degree of success, for other physical systems in whose description Lyapunov exponents play a prominent role.

#### ACKNOWLEDGMENTS

S.L.A.d.Q. thanks the Rudolf Peierls Centre for Theoretical Physics, Oxford, where this work was initiated, for the hospitality, and CNPq and Instituto do Milênio de Nanociências-CNPq for funding his visit. R.B.S. wishes to thank Alexandre Lefevre for discussions of fundamental aspects concerning the Fokker-Planck description used here. The research of S.L.A.d.Q. was partially supported by the Brazilian agencies CNPq (Grant No. 30.0003/2003-0), FAPERJ (Grant No. E26-152.195/2002), and Instituto do Milênio de Nanociências-CNPq. R.B.S. acknowledges partial support from EPSRC Oxford Condensed Matter Theory Programme Grant EP/D050952/1.

\*sldq@if.ufrj.br

†stinch@thphys.ox.ac.uk

- <sup>1</sup>H. Risken, *The Fokker-Planck Equation: Methods of Solutions and Applications*, Springer Series in Synergetics, 2nd ed. (Springer, Berlin, 1996).
- <sup>2</sup>O. N. Dorokhov, JETP Lett. **36**, 318 (1982).
- <sup>3</sup>O. N. Dorokhov, Sov. Phys. JETP **58**, 606 (1983).
- <sup>4</sup>P. A. Mello, P. Pereyra, and N. Kumar, Ann. Phys. (N.Y.) **181**, 290 (1988).
- <sup>5</sup>A. M. S. Macêdo and J. T. Chalker, Phys. Rev. B **46**, 14985 (1992).
- <sup>6</sup>D. Endesfelder, Phys. Rev. B **53**, 16555 (1996).
- <sup>7</sup>C. W. J. Beenakker, Rev. Mod. Phys. **69**, 731 (1997).
- <sup>8</sup>P. W. Brouwer, C. Mudry, B. D. Simons, and A. Altland, Phys. Rev. Lett. **81**, 862 (1998).
- <sup>9</sup>P. W. Brouwer, A. Furusaki, C. Mudry, and S. Ryu, Oyo Butsuri **60**, 935 (2005) (in Japanese).
- <sup>10</sup>D. C. Mattis, Phys. Lett. **56A**, 421 (1976).
- <sup>11</sup>D. Sherrington, J. Phys. C **10**, L7 (1977).
- <sup>12</sup>D. Sherrington, J. Phys. C **12**, 5171 (1979).
- <sup>13</sup>W. Y. Ching, K. M. Leung, and D. L. Huber, Phys. Rev. Lett. **39**, 729 (1977).
- <sup>14</sup>W. Y. Ching and D. L. Huber, Phys. Rev. B **20**, 4721 (1979).
- <sup>15</sup>R. B. Stinchcombe and I. R. Pimentel, Phys. Rev. B **38**, 4980 (1988).
- <sup>16</sup>I. R. Pimentel and R. B. Stinchcombe, Europhys. Lett. **6**, 719 (1988).

<sup>17</sup>V. Gurarie and A. Altland, J. Phys. A **37**, 9357 (2004).

- <sup>18</sup>S. L. A. de Queiroz and R. B. Stinchcombe, Phys. Rev. B **73**, 214421 (2006).
- <sup>19</sup>B. I. Halperin and W. M. Saslow, Phys. Rev. B **16**, 2154 (1977).
- <sup>20</sup>S. N. Evangelou and A. Z. Wang, J. Phys.: Condens. Matter **4**, L617 (1992).
- <sup>21</sup>A. Boukahil and D. L. Huber, Phys. Rev. B **40**, 4638 (1989).
- <sup>22</sup>I. Avgin and D. L. Huber, Phys. Rev. B **48**, 13625 (1993).
- <sup>23</sup>A. Crisanti, G. Paladin, and A. Vulpiani, in *Products of Random Matrices in Statistical Physics*, Springer Series in Solid State Sciences Vol. 104, edited by H. K. Lotsch (Springer, Berlin, 1993).
- <sup>24</sup>P. Grassberger, R. Badii, and A. Politi, J. Stat. Phys. **51**, 135 (1988).
- <sup>25</sup>H. D. I. Abarbanel, R. Brown, and M. B. Kennel, J. Nonlinear Sci. **1**, 175 (1991).
- <sup>26</sup>C. Amitrano and R. S. Berry, Phys. Rev. E **47**, 3158 (1993).
- <sup>27</sup>A. Prasad and R. Ramaswamy, Phys. Rev. E **60**, 2761 (1999).
- <sup>28</sup>S. Datta and R. Ramaswamy, J. Stat. Phys. **113**, 283 (2003).
- <sup>29</sup>J.-L. Pichard and G. Sarma, J. Phys. C **14**, L127 (1981); **14**, L617 (1981).
- <sup>30</sup>J. Hori, *Spectral Properties of Disordered Chains and Lattices* (Pergamon, Oxford, 1968).
- <sup>31</sup>W. Press, B. Flannery, S. Teukolsky, and W. Vetterling, *Numerical Recipes in Fortran; The Art of Scientific Computing*, 2nd ed. (Cambridge University Press, Cambridge, 1994), Chap. 14.